FIZIKA 9 (1977) Supplement 3, 183–214
(Proceedings of the Int. Symp. on Nuclear Collisions and
Their Microscopic Description, Bled, September 1977)

Microscopic Studies of Interaction between Composite Nuclei

Akihiro TOHSAKI-SUZUKI, Katsuyuki NAITO*, Tomoaki ANDO**
and Kiyomi IKEDA**

Faculty of Textile Science and Technology, Shinshu University, Ueda, Japan.

Introduction

Microscopic study of interaction between complex nuclei has been developed rapidly[1]. The theory has contained three basic difficulties on physical meaning: the first is the inseparability of the c.m. motion in the traditional generator coordinate space (GCM space) for the general case with different oscillator parameters, the second concerns overall saturation properties of nuclei and the last is a reflection to the relative motion from bad description of the internal states.

One of the authors (A. T-S.) proposed a new GCM space free from the c.m. motion for the general case with different oscillator parameters[2]. This space is derived by a simple procedure, which starts with the traditional GCM space and doubly Fourier transforms the GCM space to the resonating group space (RGM space) to obtain the new space. The long-time difficulty on separating the c.m. spurious motion in the GCM space is resolved by the use of the proposed space. The remaining two difficulties are untouched in this report.

* The Faculty of Liberal Arts, Shinshu University, Ueda, Japan.
** Department of Physics, Niigata University, Niigata, Japan.
+ Talk presented by A.Tohsaki-Suzuki

Furthermore, there were three serious difficulties on computational works: the first is how to construct the exchange kernels, which originate in the Pauli principle and appear in the Schrödinger's and the Hill-Wheeler's equations for many-body problem, the second how to evaluate the kernels in angular momentum representation and the last how to solve the Schrodinger's equation with ill-behaved kernels.

One of the authors (A. T-S.) developed new analytical methods of deriving the kernels, which makes skilful use of computer memory. These methods can be applied to more complex two-nucleus system with p- or sd-shell nuclei than only with s-shell one. In fact, they have been successfully used for the $^{16}O+^{16}O$ and the $\alpha+^{40}Ca$, and enable us to investigate interactions between open p-shell nuclei, such as the $^{12}C+^{12}C$. In this way the first difficulty has been overcome. On the basis of the development of the software of computer, we also evaluate the projected kernels for a simple case with one or two particle/hole directions as well as no internal direction of closed shell-nucleus system. The Schrödinger's equation has been solved by the code based on the Köhn-Hùlten and Kato's variational method, which was developed by Mito and Kamimura[3]; the code uses the new GCM kernels. All the difficulties on computational works will be overcome in the near future for the heavy ion system.

The purpose of this report is to present a picture of the microscopic theory of two-nucleus scattering and to apply the theory to typical systems.

Formulation

Starting with the harmonic oscillator shell model wave function around the parameter $\vec{R}$ of the i-th nucleus:

$$\Psi_i(\vec{R}) \propto \exp[-N_i\nu_i(\vec{r}-\vec{R})^2]\phi_i \ , \qquad (1)$$

we write the traditional GCM wave function:

$$|\vec{R}> \propto \mathcal{A}_{12}\{\Psi_1(-\frac{N_2}{N_1+N_2}\vec{R})\Psi_2(\frac{N_1}{N_1+N_2}\vec{R})\} \ , \qquad (2)$$

where ϕ_i means the internal wave function, N_i the mass number, ν_i the oscillator parameter and $\mathcal{A}_{12}$ the antisymmetrizer between two nuclei. The Hill-Wheeler equation base on Eq.(2)

$$\int <\vec{R}| H-E |\vec{R}'>f(\vec{R}')d\vec{R}' = 0 \qquad (3)$$

includes the c.m. spurious motion to be eliminated for the general case with different oscillator parameters, where $<\vec{R}|\ \hat{O}\ |\vec{R}'>$ is so-called the traditional GCM kernel. We cannot, however, directly separate the c.m. motion in Eq.(3).

Nevertheless, we can transform the traditional GCM kernel into the RGM one without the c.m. motion. The transformation procedure to the RGM kernel is presented as follows:

$$\overbrace{\hat{A}\hat{B}\ <\vec{R}|\ \hat{O}\ |\vec{R}'>\ \hat{B}\hat{A}} = <\vec{r}|\ \hat{O}\ |\vec{r}'> \ , \qquad (4)$$

where $\vec{r}$ is the dynamical variable and $<\vec{r}|\ \hat{O}\ |\vec{r}'>$ the RGM kernel with local part described by the δ-function., which composes the

$$\int \langle \vec{r} | \; H-E \; | \vec{r}' \rangle \chi(\vec{r}') d\vec{r}' = 0 \; . \qquad (5)$$

The operator $\hat{B}$ transforms the traditional GCM kernel into the momentum space one, $\hat{A}$ it to the RGM one and the symbol $\overbrace{\quad}$ also means the inseparability of $\hat{A}\hat{B}$ between bla and ket for the general case. Several authors pointed out the relation of Eq.(4) from some angles; the combination of $\hat{A}$ with $\hat{B}$ for the case with common oscillator parameter is called the "separable double Fourier transform"[4,5] and the kernel $\hat{B}\langle\vec{R}|\; \hat{O} \; |\vec{R}'\rangle\hat{B}$ is treated as the "complex GCM kernel"[6,7].

On the other hand, the GCM kernel without the c.m. motion is regarded as the superposition of the RGM one with a weight. The new GCM kernel is written as

$$\hat{C} \langle \vec{r} | \; \hat{O} \; | \vec{r}' \rangle \; \hat{C} = \langle \vec{S} | \; \hat{O} \; | \vec{S}' \rangle \quad , \qquad (6)$$

where the parameter $\vec{S}$ generates the relative motion without the c.m. motion. The operator $\hat{C}$, for example, is assumed to be that of the Gauss weight function.

As soon as we write down an analytical formula of the traditional GCM kernel, we can derive the RGM and the new GCM ones by the use of Eqs.(4) and (6). If the analytical formula is given by

$$\exp(-E_1 R^2 - E_2 R'^2 + E_3 \vec{R}\cdot\vec{R}') \qquad (7)$$

for the traditional GCM kernel, the RGM and the new GCM ones are

obtained by

$$D\, C_0^{-3/2} \exp[-\frac{1}{C_0}(C_1 r^2 + C_2 r'^2 - C_3 \vec{r}\cdot\vec{r}')] \ , \tag{8}$$

$$P_0^{-3/2} \exp[-\frac{1}{P_0}(P_1 S^2 + P_2 S'^2 - P_3 \vec{S}\cdot\vec{S}')] \ , \tag{9}$$

respectively. Here the parameters C_0, P_0 and others are determined by the combinations of E_1, E_2, E_3, ν_1 and ν_2. The Gauss function formula of the kernel is general, if the interanal wave function is adopted as the harmonic oscillator type.

Comparison between Eqs.(7) and (9) leads to estimation of the c.m. motion in the traditional GCM kernel. It is clear from such comparison that the mixture of the c.m. motion makes nonlocality of the kernel increase and originates in the antisymmetrization and in the nucleon-nucleon interaction; but the effect of the antisymmetrization is stronger than the effect of another one.

At last we need present how to construct the traditional GCM kernel in the analytical formula, which is indispensable for the derivation procedure of other two kernels. There are two main algolithms in computer technique: one is called the "Rendez-Vous program, which makes use of the orthogonality of the Herimete polynomial and another is computer code the "UFPN", which is based on method of general algorithm on unique factorization by the analytical use of computer memory. Contents of such codes will be reported in Prog. Theor. Phys. Suppl. in the near future.

$^{16}O+^{16}O$ interaction

We analyze the RGM equation with correct boundary condition of scattering problem. Tanabe, Tamagaki and one of the authors (A. T-S.)[5] solved the RGM by the step-by-step method and Suzuki and two of the authors[8] within the bound-state approximation without the Coulomb interaction kernel. The present calculation are progressed as taking into account the accurate kernel at very small distance with origin and are performed by the use of computer code "VAR-GCM" based on the variational method, which was developed by Mito and Kamimura[3]. The qualitative features are slightly revised from the previous results. In this calculation, we adopt mainly the Volkov. No.2[9] with m=0.65 as nucleon-nucleon interaction and the oscillator parameter $\nu_0=0.195fm^{-2}$ to satisfy the saturation property of ^{16}O nucleus, which leads to $\hbar\omega=16.2MeV$.

The energy surfaces in the GCM space have the rotational feature corresponding to the gross structure peaks as exhibited in Fig.1. The phase shifts δ_ℓ(real) are shown Fig.2. The main features of δ_ℓ are similar to those obtained from a phenomenological potential of Yale group[10]. These results indicate that the RGM is expected to provide a realistic description of the real part of optical potential if a suitable nucelon-nucleon interaction is adopted. Also the energy eigenvalues and the resonance energies E_ℓ(res) defined by $\delta_\ell(E_\ell)=90°$ show the good correspondence with the energy minima E_ℓ(min) as illustrated in Fig1. But the second rotational series show the similar feature to the lowest ones; therefore the gross structure peaks may correspond to the second series for the deep energy surfaces by the use of two-nucleon interaction with small m=0.63. The difference may lead

to the similar problem from the microscopic situation as whether shallow or deep for the phenomenological nucleus-nucleus potential.

In Fig.3, the relative wave functions are shown for the lowest eigenvalue of $\ell=0$. Here, three wave functions are defined by

$$\tilde{\chi} = \Lambda\chi \quad \text{with} \quad \Lambda = 1 - \sum_{i} \chi^{(i)}\rangle\langle\chi^{(i)} \quad , \tag{10}$$

$$\psi = F\chi \quad \text{with} \quad F = \langle\vec{r}|\vec{r}'\rangle^{1/2} \quad , \tag{11}$$

$$U = \langle\vec{r}|\vec{r}'\rangle\chi \quad , \tag{12}$$

where $\chi^{(i)}$ is the well-known redundant solustion. The operator $\langle\vec{r}|\vec{r}'\rangle$ is expanded as

$$\langle\vec{r}|\vec{r}'\rangle = \sum_{j(\text{all})} \mu_j \chi^{(j)}\rangle\langle\chi^{(j)} \quad . \tag{13}$$

The forbidden states with $\mu_j=0$ are automatically eliminated in the three functions. As shown by Saito, Okai, Tamagaki and Yasuno[11], ψ obeying the usual normalization is suitable as the relative wave function. For the light clusters, three representations are essentially the same because of $\mu_j(\text{non-redundant})\sim 1$. In the $^{16}O+^{16}O$, however, there are a lot of almost forbidden states as shown in Fig.3. From the present calculation with nucleon-nucleon interaction to fulfill the saturation property of ^{16}O nucleus, ψ and U have the following different features from $\tilde{\chi}$:

(i) the inner oscillation is strongly damped reflecting the important role of the Pauli principle through the almost forbidden states. This property physically indicates the existence of a hard-core-like potential in the innermost region

(ii) Many non-redundant solutions shift the outer wave to larger separation by ∿0.5fm. These characteristic feature cannot be reproduced simply by artificial increase of the number of the orthogonal conditions.

Recently, Buck et al.[12] discussed about an importance of the dynamical effect for strong damping of the inner oscillations by using the model interaction of the harmonic oscillator type. We, in detail, analyze this effect from viewpoint of nuclear saturation properties by using the Volkov No.2 with variable Majorana parameter. The results are exhibited in the follwing for the typical case with m=0.60, 0.65 and 0.70. The oscillator parameter is chosen to give a minimum energy of ^{16}O for each case. The energies are fixed on the basis of the $^{16}O+^{16}O$ threshold one; they are adjusted as $E_0(\infty)$ for all the cases. In Fig.4, the energy surfaces for $\ell=0$ are shown , together with eigenvalues of the lowest states, which are -43.7, -2.4 and 11.3Mev for m=0.60, 0.65 and 0.70, respectively, For m=0.60 the minimum energy and also the lowest eigenvalue unrealistically exceeds the lower bound of the empirical ground state energy of E_0=-16.65MeV for ^{32}S.

It is important for the present consideration to see the relative relation of the saturation energies between the compact ^{32}S and the $^{16}O+^{16}O$. We assume the configuration of $[(sd)^{16}$ [4444] $(\lambda\mu)=(48)$, $J^\pi=0^+]$ as the wave function of ^{32}S. The calculated energy of this state is shown in Table I, together with the limiting energy of $E_0(R=0)$ and also with the lowest eigen energy for each case, where $E_0(R=0)$ is known to represent the energy of $4\hbar\omega$ excited state involved in the model wave function of $\mathcal{A}_{12}\{\phi_1\phi_2\chi\}$. It should be noted that for m=0.70 the energy of the compact ^{32}S is

higher than the lowest eigenvalue of the $^{16}O+^{16}O$ and on the other side the binding energy of the ground state is too large for m=0.60. Only the case with m=0.65 satifies the relative relation of the empirical saturation properties.

Next we exhibit the relative wave function ψ of the lowest eigenstate for three cases in Fig.5. It is seen that the inner oscillation damps strongly in comparison with $\alpha+\alpha$ and $\alpha+^{16}O$ cases for all three cases. For the case with m=0.60, the amplitude of the inner oscillation increases appreciably and the wave function is shrinkage due to the unnaturally strong interaction energy. On the other hand, the inner amplitude is vanishingly small for the case with m=0.70 because of the scanty of the binding energy for the compact ^{32}S system.

Thus we understand that as far as the relative relations of the saturation properties between the compact system and the separated system are satisfied as seen in the case with m=0.65, the inner oscillation is very small and simultaneously the well developed cluster state is obtained as a loosely bound or a quasibound state. The ψ for the scattering state is illustrated for two cases in the right side of Fig.5. The study for the higher partial waves upto ℓ=30 is also performed and the results for higher ℓ are almost same for ℓ=0. Then it seems that the concept of the inner core potential is accepted for the interaction between p-shell nuclei.

$\alpha+^{40}Ca$ system

Transient phenomena from the "shell" phase into the "cluster" one has been investigated in the region of ^{20}Ne nucleus[13,14]. Several authors have considered either the model including decomposition of the ^{16}O core[13] or taking account of the other symmetries adding to the [4]-symmetry[14]. Another approach is to treat the two-cluster system with different oscillator parameters; this approach can include new states which are eliminated as the redundant solutions in the case with common oscillator parameter. For the $\alpha+^{40}Ca$ system, the main purpose of this section is to give a relation between the "shell" and the "cluster" phases by this approach.

Let us see the behavior of the norm kernel as focussing the c.m. motion in the traditional GCM kernel, before investigating the dynamical study of the RGM. If the internal wave functions α and ^{40}Ca are assumed to be $(0s)^4$ and $(0s)^4(0p)^{12}(1s0d)^{24}$ of L-S coupling shell model, the traditional GCM kernel is obtained by the straightforward calculations of 4-power of determinant. In order to conserve the quantum number, the quantity $(\nu_\alpha-\nu_{Ca})/(\nu_\alpha+\nu_{Ca})$ plays the same role as the relative quantum number; therefore the breathing mode is treated in this scheme, which changes the size of nucleus during scattering process.

The new space kernel is derived by the procedure mentioned in the section of formulation, cannot hold the separable type divided in the product of the matrix elements between one-nucleon wave functions and also cannot hold 4-power of the determinant. To evaluate the c.m. motion in the traditional GCM kernel, we introduce the harmonic expansion in the dynamical space for the

kernels. The expansion coefficient for the traditional GCM kernel $\mu^{R}_{nn'}$ includes the quantity coming from the c.m. spurious motion. The degree of the c.m. motion is evaluated by the subtraction of the coefficient of the new GCM kernel $\mu^{S}_{nn'}$ from $\mu^{R}_{nn'}$. In the special case with common oscillator parameter the diagonal parts of $\mu^{R}_{nn'}$ are just the eigenvalues and are independent of the angular momentum ℓ. In the present calculation, the oscillator parameters are assumed to be those of free nuclei, that is, $\nu_{\alpha}=0.28\text{fm}^{-2}$ and $\nu_{Ca}=0.14\text{fm}^{-2}$. The diagonal parts and eigenvalues of both the cases are exhibited in Table II and the eigenvalues of $\mu^{S}_{nn'}$ corresponding to each ℓ are listed in Table III. The following characteristic features are clear from these Tables:

(i) The c.m. motion in the traditional GCM kernel becomes extremely larger in the range of $N=2n+\ell<12$. The diagoanl parts include the c.m. motion of 28% for $N=0$ ($\ell=0$) and 25% for $N=1$ ($\ell=1$). In such range of N the matrix elements $\mu^{S}_{nn'}$ have large non-diagonal parts. The eigenvalues depend on the angular momentum and become the smallest for the highest ℓ in allowed ℓ for the common N, except for the case with small N. The region $N<12$ leads to forbidden one in the case with common oscillator parameter.

(ii) On the other hand, the c.m. motion is small for the kernel with larger components with $N>12$. The angular momentum dependence is also small for such region of N.

(iii) The deviation of the eigenvalues from the case with common oscillator parameter are still large for the states with $N\geq 12$. The eigenvalue with main component of $N=12$ ($\ell=0$) is 0.1123 , which 160% for the corresponding case with common oscillator parameter.

We emphasize from these results that the c.m. spurious motion affects the traditional GCM kernel in short range, where it is mixed by many particle-exchanges originating in the antisymmetrization.

Next we solve the RGM equation within the bound-state approximation without the Coulomb interaction kernel. We show the level schemes in Fig.6, where the oscillator parameter ν_{Ca} is fixed as $0.14fm^{-2}$ and ν_{α} is variable. As the nucleon-nucleon interaction we adopted the Brink-Boker B1 force[15] for all the cases and the Volkov No.2 with m=0.70 (denoted as V2) for the case with common oscillator parameter. In the case with common oscillator parameter the antistretching effect strikingly appears for ℓ=10 and 12 states of the ground band. This effect free from the choices of the nucleon-nucleon interaction. Numerical results show that the second rotational band with ℓ=10 and 12 reaches smmothly to the first state of ℓ=14. Kihara, Kamimura and two of the authors (A. T-S. and K. N.) are investigating this effect and the structure of ^{44}Ti with further calculation of B(E2) and behavior of phase shifts including the Coulomb interaction kernel. Friedrich and Langanke[16] indicated that the anyistretch appears for ℓ=10 and 12. They analyzed the RGM equation by the use of the numerical transformation from the numerical values of the GCM kernels and mentioned that the antistretch is caused by the behavior of the kernels at small distances. Their numerical calculation was, however, performed without using the kernels in this region. On the other hand, the present calculation is accurate in this region because of the harmonic expansion of the kernels.

The case with different oscillator parameters prevents the ℓ=10 and 12 states from the antistretch; since the barrier between two nuclei is strikingly generated, the pure rotational band

appears as shown in Fig.6. This barrier can be illustrated by the energy surfaces versus distance parameter R; here the c.m. spurious motion is eliminated. Fig.7 shows the non-projected energy surfaces for three cases with ν_α/ν_{Ca}=1, 1.5 and 2. The barrier around R∿3fm becomes higher and the inner minimum lower; the barrier is the highest for the limiting case with $\nu_\alpha \to \nu_{Ca}$ ($\nu_\alpha \neq \nu$) and behaves like a core-pulse. The wave function corresponding to the inner minimum may be $(1p0f)^4$ [4]-shell model states except for the (12,0) SU_3 state. This barrier disappears for ℓ=14, which has no forbidden state in the case with common oscillator parameter. Though Sunkel's calculation[17] showed an anomalous effect for ℓ=7 and 8 states with a modified SW force, our caculation with BL force does not generate such anomaly. In conclusion, a kind of new core potential, which divides the $\alpha+^{40}Ca$ interaction into two regions, appears for the case with different oscillator parameters; the inner region corresponds to the "shell" phase and the outer to the "cluster" one.

$^{12}C+^{12}C$ system

In this section we propose a comprehensive model of the $^{12}C+^{12}C$ system; in addition to the elastic channel, the model contains the other channels with rearrangement reactions, such as $\alpha+^{20}Ne$ and $^{8}Be+^{16}O$. We also consider a role of a hypothetic channel during the scattering process. For example, an introduction of $^{12}C+^{12}C^*$ (loosely dounded 3α-state) may give an important path from $^{12}C+^{12}C$ channel to other ones. As the first step of this scheme, we treat the system in non-projected problem.

We assume configuration shown in Fig.8(a) as the intrinsic state of $^{12}C+^{12}C$ system, which transfers SU_3 (84)-state of ^{24}Mg as

the limiting case with inter-nucleus distance R→0 and α-α one in ^{12}C d→0. As ^{8}Be configuration we adopt the superposition of two directions of α+α, which are parrarel to the scattering axis and perpendicular to one aA illustrated in Fig.8(c). The ^{16}O nucleus traps one α-particle in ^{8}Be along the scattering axis and then the ^{20}Ne nucleus is produced as shown in Fig.8(d). Also if the ^{12}C nucleus smiltaneously traps two α-particles in another ^{12}C, ^{20}Ne is produced again. But this reaction is strong in short range, where the compound process is dominant. Then we can ignore the reaction because of the same description as the $^{8}Be+^{16}O$ in this region.

Overlapping matrix elements between different channels shows dominant components in small region. Therefore, α-partcle shell model proposed by Michaud and Vogt[18] may be good picture for the molecular resonaces. We cannot, however, distingush their model from the compound nucleus one . If we introduce the hypothetic channel as intermediate system, can you indicate another aspect for molecular resonaces? As this system, we take a schematic model of $^{12}C+^{12}C^{*}$ as illustrated in Fig.8(b) on the basis of recent studies of individual ^{12}C nucleus, which have reavealed the structure of the second 0^{+} state from the microscopic calculation[19,20,21]. This state consists of 3α-particles loosely bounded; we take into account the simplest configuration of the superposition of the linear and the isoscales tranqle ones. It is possible that the $^{12}C+^{12}C$ transiates other channels through the hypothetic channel. Futhermore, this system produces the closed "^{16}O nucleus" during scattering process in large distance and gains large binding energy. Such intermediate channel enables us to give two aspects for the molecular resonances from the microscopic viewpoint.

In order to estimate the coupling effects between different channels through a simple picture, we introduce the following potentials in the two ways: one is the "slow" potential and another the "fast" potential proposed by Greiner[22]. These potentials are represented in the GCM space through the kernels. The slow potential is defined by the diagonalization for the systems at fixed R and the fast potential is given by the energy surfaces of each system; the slow potential decribes the low energy phenomena and the fast one the high energy phenomena.

In the present calculations, we adopt $0.19fm^{-2}$ as the common oscillator parameter for all the systems. The nucleon-nucleon interaction is assumed to be Volkov No.2 with m=0.65. The coupled channel equation in the GCM space is solved within the bound-state approximation including exact Coulomb energy kernel and mesh points for R are 2, 3, 4, 5, 6, 7fm, which cover the overall interaction region.

The norm kernels between different systems are illustrated in Fig.9. The case between the $^{12}C+^{12}C$ and the $\alpha+^{20}Ne$ is omitted because of the approximate orthogonality, where the value is smaller than 10^{-3} over wide region. This is due to less transition between the triangle and the linear 3α configurations in quasi ^{12}C. Either the rotation of a ^{12}C in one incident channel or that of ^{20}Ne in another one leads to larger coupling at short range; but the transition at such region may be regarded as a compound process.

The case between the $^{12}C+^{12}C$ and the $^{8}Be+^{16}O$ shows the strong overlapping at small distance around $\sim$3fm, where the anti-symmetrization plays a major role. On the other hand, there are two local maxima between the $^{8}Be+^{16}O$ and the $\alpha+^{20}Ne$ near the origin and

at large range. The outer narrow peak may spread to the bottom; a path opens to the $\alpha+^{20}Ne$ at common distance with the maximum point of the norm kernel between the $^{12}C+^{12}C$ and the $^{8}Be+^{16}O$; neverthless the path leads to the compound process.

Let us pay our attention to the norm kernel with the $^{12}C+^{12}C^{*}$. This channel has the strong overlapping with all other ones, which is larger than 0.1. In addition, there are the following features: The figure shows two local maxima for all the cases, which is reflected from the behavior of such channel. The striking repulsive core appears for this channel, which is represented in the fast potential; when an α-particle in the $^{12}C^{*}$ passes through another ^{12}C, this barrier generates. The inner maximum describes the compound process and the outer corresponds to molecular resonances. We should focuss the physical quatities concerning the outer maximum.

We show the slow and the fast potentials. Since the binding energy of the ^{12}C cannot be reproduced from the usual two-nucleon interaction, the fast potentials of the $^{12}C+^{12}C$ and the $^{12}C+^{12}C^{*}$ start at higher energy than experiments. Such two curves drop down rapidly (See Fig.10), and are comparable to other ones. It is important to indicate that the $^{12}C+^{12}C^{*}$ crosses the $^{12}C+^{12}C$ around $\sim$8fm. The outer minimum appears in the $^{12}C+^{12}C^{*}$ at 5fm; at such region this system composes a stable ^{16}O during scattering process. process. Though the $^{12}C^{*}$ is excited state of 7.2MeV in individual nucleus, it happens that the system with the $^{12}C^{*}$ is more stable than with the ground state configuration of ^{12}C.

Corresponding to the cross of the fast potentials and to the behavior of the norm kernels, the slow potentials shows th following feature: There is small dip in the lowest potential around 7fm in

realtion between the $^{8}Be+^{16}O$ and the $\alpha+^{20}Ne$. The slow potentials are seriously different from the fast one. We can appreciate the strong coupling at large range, where nuclear molecule is composed.

We solve the equation with a correlation function, which is the aim of reproducing all the threshold energies and does not affect small distance; the correlation function is reflected from the norm kernel. At first we show each level scheme without the coupling in the right side of Fig.11. For the $^{12}C+^{12}C$, the second nodal band appears near the Coulomb barrier, where typical resonances are observed[23]. The ground state of ^{24}Mg is estimated by the diagonalization of the $^{8}Be+^{16}O$; the $\alpha+^{20}Ne$ and the $^{12}C+^{12}C$ also reach to the ground state configuration as the ^{20}Ne rotates and the α-α distance in the ^{12}C approaches to 0fm. Dynamical treatment of further suitable variable may decrease the binding energy of 24-body system and descrives an appropriate ground state of ^{24}Mg.

Three cases of the coupled channel GCM are lined in the left side of Fig.11. The first is solved within all the channels, the second except for the $^{12}C+^{12}C^{*}$ for comparison and the last within two channels concerning the two ^{12}C nuclei. The first two cases indicate almost the same result for the low-lying levels, which show the level schemes of ^{24}Mg in this model and the last does not reproduce such levels because of bad configuration at small distance.

There is , however, the difference between the first two cases near and over the Coulomb barrier of the $^{12}C+^{12}C$ (the arrow A indicates it). In interesting levels marked in Fig., we consider the behavior of the modified weight function free from redundancy. The level 1, 3 and 4 have common property; there is domminant component of the $^{8}Be+^{16}O$, and the $^{12}C+^{12}C^{*}$ takes the place of the $^{8}Be+^{16}O$ for the level 4 (See Fig.12). The $^{12}C+^{12}C$ also plays a role

in these levels. The increase of the diagonalization number decrease the energy level, which reaches to the level 1. However, the $\alpha+^{20}Ne$ plays a minor role in these levels.

The level 2 has the more characteristic feature than that mentioned above. All the channels have considerable components at large distance. Abobe all the $^{12}C+^{12}C^{*}$ gives the dominance due to the outer minimum of the fast potential. This level coming from the hypothetic system make a important path from the $^{12}C+^{12}C$ to other channels.

We expect someone further investigation on realistic two-nucleon interaction for the heavy ion system. On the basis of this, it is hopeful method to perform the microscopic calculation on the proposed scheme with the $^{12}C+^{12}C^{*}$ and to solve the scattering problem with correct boundary condition by the use of the kernel in angular momentum representation.

This work was performed as an annual research project on "Highly Excited States in Nuclei and Molecular Resonances" organized by Research Institute for Fundamental Physics, Kyoto University, in 1976 and 1977. All the members of the project are acknowledged. The authors would like to thank Prof. R. Tamagaki for valuable discussions and constant encouragement.

References

1) Proc. INS-IPCR Int. Symp. on Cluster Structure of Nuclei and Transfer Reactions Induced by Heavy Ions, Tokyo (1975). Proc. II Int. Conf. on Clustering Phenomena in Nuclei, Maryland (1975).

2) A. Tohsaki-Suzuki, preprint.

3) Y. Miyo and M. Kamimura, Prog. Theor. Phys. 56 (1976), 583.

4) B. Giraud and J. LeTourneux, Nucl. Phys. A197 (1972), 410.

5) A. Tohsaki, F. Tanabe and R. Tamagaki, Prog. Theor. Phys. 53 (1975), 1022.

6) H. Horiuchi, Prog. Theor. Phys. 50 (1973), 529.

7) D. R. Thompson, M. LeMere and y. c. Tang, Phys. Letters 69B (1977), 1.

8) T. Ando, K. Ikeda and Y. Suzuki, Prog. Theor. Phys. 54 (1975), 119.

9) A. B. Volkov, Nucl. Phys. 74 (1965), 33.

10) J. V. Maher, M. W. Sachs, R. H. Siemssen, A. Weidinger and D. A. Bromley, Phys. Rev. 188 (1969), 1665.

11) S. Saito, S. Okai, R. Tamagaki and M. Yasuno, Prog. Theor. Phys. 50 (1973), 1561.

12) B. Buch, H. Friedrich and C. Wheatley, Nucl. Phys. A275 (1977), 246.

13) F. Nemoto, Y. Yamamoto, H. Horiuchi, Y. Suzuki and K. Ikeda, Prog. Theor. Phys. 54 (1975), 104.

14) T. Tomoda and A. Arima, page 60 of the first of Ref. (1).

15) D. M. Brink and E. Boeker, Nucl. Phys. A91 (1967), 1.

16) H. Friedrich and K. Langanke, Nucl. Phys. A252 (1975), 47.

17) W. Sunkel, Phys. Letters 65B (1976), 419.

18) G. Michaud and E. W. Vogt, Phys. Rev. C5 (1972), 350.

19) Y. Fujiwara and R. Tamagaki, Prog. Theor. Phys. 56 (1976), 1503.

20) E. Uegaki, S. Okabe, Y. Abe and H. Tanaka, Prog. Theor. Phys. 57 (1977), 1262.

21) Y. Fukushima ans M. Kamimura, contribution paper to 1977' Tokyo Cof. on Nuclear Structure.

22) K. Pruess and W. Greiner, Phys. Letters 33B (1970), 1970.

23) E. Almqvist, D. A. Bromley and J. A. Kuehner, Phys Letters 4 (1960), 515.

Table I Energy relations between the oergate ^{32}S and the ^{16}O-^{16}O system.

	m=0.60, =0.235fm^{-2}	m=0.65, =0.195fm^{-2}	m=0.70, =0.165fm^{-2}	EXPERIMENT
^{32}S GROUND	-76.3 MeV	-8.5 MeV	31.5 MeV	-16.6 MeV
E_0 (EIGENVALUE)	-43.7 MeV	-2.4 MeV	11.3 MeV	----
E_0 (R=0)	-24.2 MeV	37.9 MeV	73.1 MeV	----

Table II Diagonal parts and eigenvalues for the norm kernel of the $\alpha+^{40}Ca$. $\mu^{R}_{nn'}$ includes the c.m. spurious motion.

$\ell=0$		$\mu^{S}_{nn'}$		$\mu^{R}_{nn'}$	
N	$\nu_\alpha = \nu_{Ca}$	Diagonal Parts	Eigen Values	Diagonal Parts	Eigen Values
0		$.1927\cdot10^{-6}$	$.1580\cdot10^{-6}$	$.2461\cdot10^{-6}$	$.2103\cdot10^{-6}$
2		$.2798\cdot10^{-4}$	$.6685\cdot10^{-5}$	$.3219\cdot10^{-4}$	$.7118\cdot10^{-5}$
4		$.1381\cdot10^{-2}$	$.3433\cdot10^{-4}$	$.1398\cdot10^{-2}$	$.3847\cdot10^{-4}$
6		$.1665\cdot10^{-1}$	$.2892\cdot10^{-3}$	$.1668\cdot10^{-1}$	$.3178\cdot10^{-3}$
8		$.7790\cdot10^{-1}$	$.2768\cdot10^{-2}$	$.7836\cdot10^{-1}$	$.2980\cdot10^{-2}$
10		.1908	$.2202\cdot10^{-1}$	.1918	$.2319\cdot10^{-1}$
12	$.6914\cdot10^{-1}$	.3090	.1124	.3104	.1157
14	.2641	.4184	.2896	.4196	.2917
16	.4751	.5150	.4794	.5166	.4802
18	.6479	.6025	.6395	.6041	.6395
20	.7728	.6823	.7593	.6834	.7590
22	.8571	.7527	.8433	.7533	.8429
24	.9117	.8121	.8998	.8122	.8994
26	.9462	.8601	.9368	.8599	.9365
28	.9676	.8975	.9607	.8971	.9604
30	.9806	.9258	.9760	.9254	.9758
$\ell=1$					
1		$.2436\cdot10^{-5}$	$.1547\cdot10^{-5}$	$.3034\cdot10^{-5}$	$.1916\cdot10^{-5}$
3		$.2268\cdot10^{-3}$	$.1309\cdot10^{-4}$	$.2426\cdot10^{-3}$	$.1410\cdot10^{-4}$
5		$.4939\cdot10^{-2}$	$.9950\cdot10^{-4}$	$.5113\ 10^{-2}$	$.1090\cdot10^{-3}$
7		$.3754\cdot10^{-1}$	$.8103\cdot10^{-3}$	$.3811\cdot10^{-1}$	$.9167\cdot10^{-3}$
9		.1287	$.6611\cdot10^{-2}$	.1297	$.7513\cdot10^{-2}$
11		.2497	$.4331\cdot10^{-1}$	.2509	$.4722\cdot10^{-1}$
13	.1573	.3646	.1924	.3660	.1954
15	.3723	.4650	.3858	.4668	.3873
17	.5675	.5564	.5641	.5583	.5645
19	.7161	.6412	.7043	.6427	.7041
21	.8193	.7178	.8052	.7187	.8049
23	.8875	.7836	.8744	.7839	.8740
25	.9310	.8376	.9203	.8375	.9199
27	.9582	.8802	.9500	.8799	.9497
29	.9749	.9129	.9690	.9124	.9683
31	.9851	.9373	.9813	.9368	.9811

Table III Eigenvalues for the norm kernel run from ℓ=0 to 13.

N	$\nu_R = \nu_{CA}$	ℓ = 0	2	4	6	8	10	12
0		$.1580\cdot10^{-6}$						
2		$.6685\cdot10^{-5}$	$.9303\cdot10^{-5}$					
4		$.3433\cdot10^{-4}$	$.3717\cdot10^{-4}$	$.5443\cdot10^{-4}$				
6		$.2892\cdot10^{-3}$	$.3090\cdot10^{-3}$	$.4123\cdot10^{-3}$	$.3021\cdot10^{-3}$			
8		$.2768\cdot10^{-2}$	$.2836\cdot10^{-2}$	$.2950\cdot10^{-2}$	$.2758\cdot10^{-2}$	$.1850\cdot10^{-2}$		
10		$.2202\cdot10^{-1}$	$.2167\cdot10^{-1}$	$.2081\cdot10^{-1}$	$.1924\cdot10^{-1}$	$.1662\cdot10^{-1}$	$.1266\cdot10^{-1}$	
12	$.6914\cdot10^{-1}$	.1124	.1117	.1100	.1073	.1034	$.9809\cdot10^{-1}$	$.9129\cdot10^{-1}$
14	.2641	.2896	.2890	.2877	.2856	.2826	.2787	.2739
16	.4751	.4794	.4790	.4782	.4768	.4750	.4726	.4696
18	.6479	.6395	.6392	.6387	.6379	.6368	.6354	.6337
20	.7728	.7593	.7592	.7589	.7585	.7578	.7570	.7561
22	.8571	.8431	.8432	.8431	.8428	.8425	.8420	.8415
24	.9117	.8996	.8997	.8996	.8995	.8993	.8991	.8988
26	.9462	.9368	.9367	.9367	.9366	.9365	.9363	.9362
28	.9676	.9607	.9605	.9605	.9604	.9604	.9603	.9602
30	.9806	.9760	.9757	.9756	.9755	.9755	.9755	.9754

N		ℓ = 1	3	5	7	9	11	13
1		$.1547\cdot10^{-5}$						
3		$.1309\cdot10^{-4}$	$.2179\cdot10^{-4}$					
5		$.9950\cdot10^{-4}$	$.1219\cdot10^{-3}$	$.1179\cdot10^{-3}$				
7		$.8103\cdot10^{-3}$	$.8838\cdot10^{-3}$	$.9271\cdot10^{-3}$	$.6904\cdot10^{-3}$			
9		$.6611\cdot10^{-2}$	$.6634\cdot10^{-2}$	$.6520\cdot10^{-2}$	$.5897\cdot10^{-2}$	$.4371\cdot10^{-2}$		
11		$.4331\cdot10^{-1}$	$.4244\cdot10^{-1}$	$.4074\cdot10^{-1}$	$.3803\cdot10^{-1}$	$.3400\cdot10^{-1}$	$.2843\cdot10^{-1}$	
13	.1573	.1924	.1915	.1896	.1869	.1832	.1783	.1722
15	.3723	.3858	.3851	.3838	.3818	.3791	.3758	.3716
17	.5675	.5641	.5637	.5628	.5616	.5600	.557	.5555
19	.7161	.7043	.7040	.7035	.7028	.7018	.7007	.6993
21	.8193	.8052	.8051	.8048	.8044	.8039	.8032	.8025
23	.8875	.8744	.8743	.8742	.8740	.8737	.8733	.8729
25	.9310	.9203	.9202	.9201	.9200	.9198	.9196	.9194
27	.9582	.9500	.9499	.9499	.9498	.9497	.9496	.9495
29	.9749	.9690	.9689	.9689	.9688	.9688	.9687	.9687
31	.9851	.9813	.9810	.9809	.9808	.9808	.9807	.9807

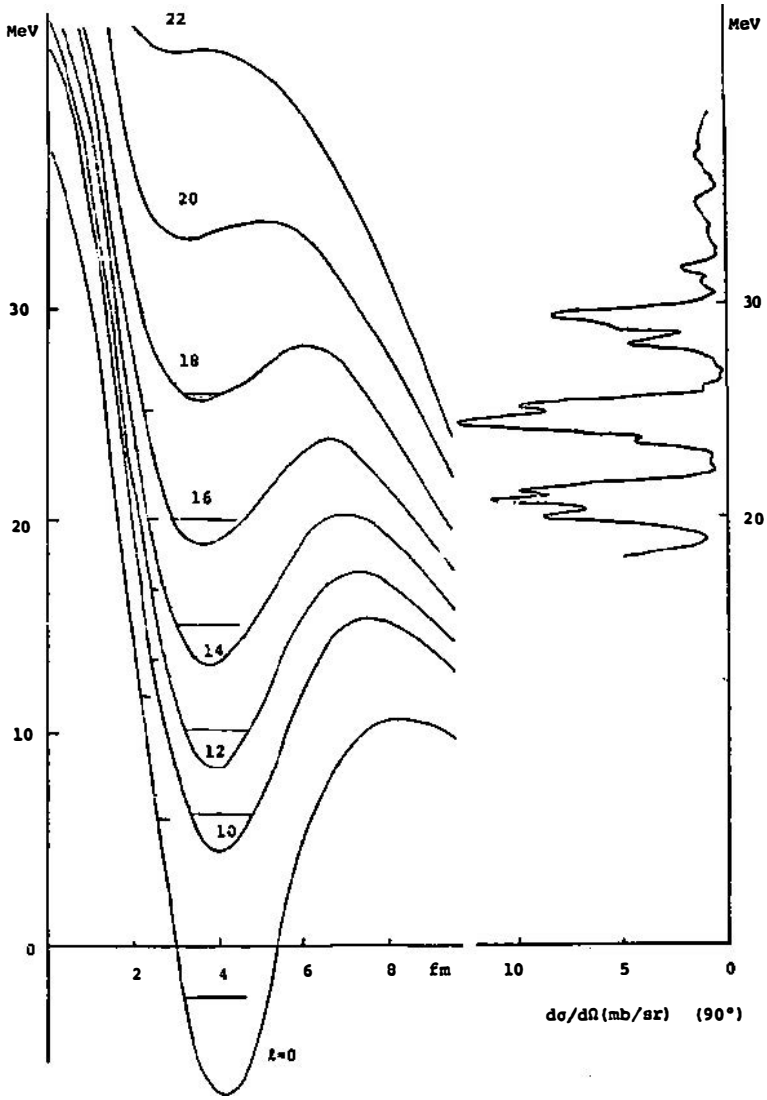

Fig.1 Energy surfaces including the Coulomb energy. The solid lines show the level positions evaluated from the energy eigenvalues and the resonances of phase shifts.

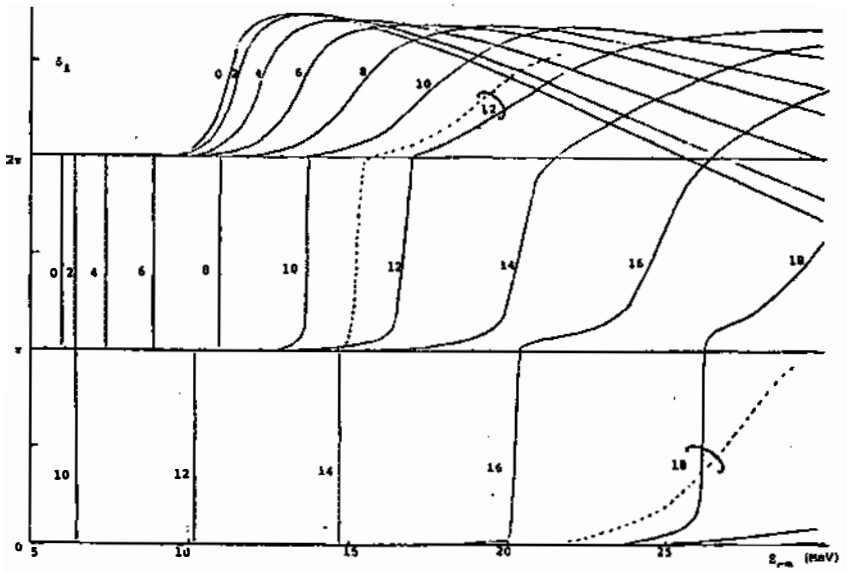

Fig.2 Real phase shifts δ_L. The dashed lines are the values calculated from the phenomenological real potential of Ref. 10

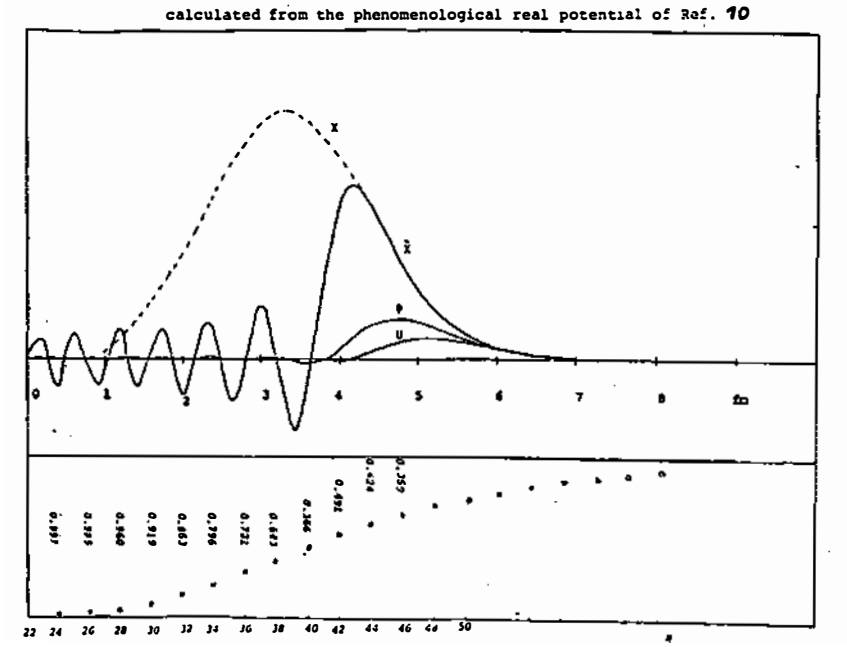

Fig.3 Eigenvalues $1-\mu_N$ and an illustrated example of effects of non-redundant solutions on the wave function for $\ell=0$. The inner oscillation of ψ and U has twelve nodes but the amplitudes are strongly damped.

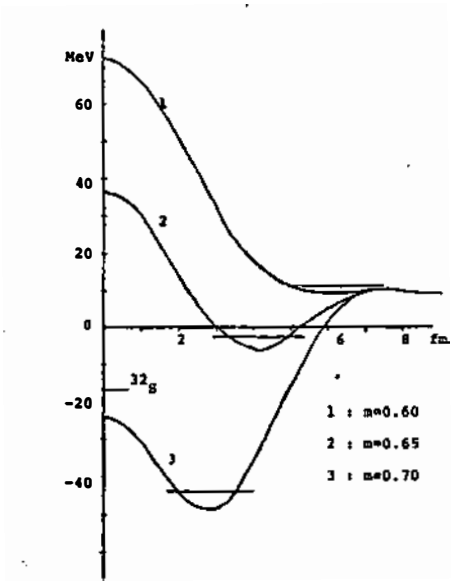

Fig. 4.

The energy surfaces for $\ell = 0$ are shown in three cases with m's. The solid lines show the energy eigenvalues corresponding to each case. The empirical energy of ^{32}S is listed on the axis of ordinates.

Fig. 5.

The wave function ψ for $\ell = 0$ is shown in the left side, where the energies correspond to those of eigenvalues. In the right side the wave functions are exhibited for the scattering state in the suitable case with m = 0.65.

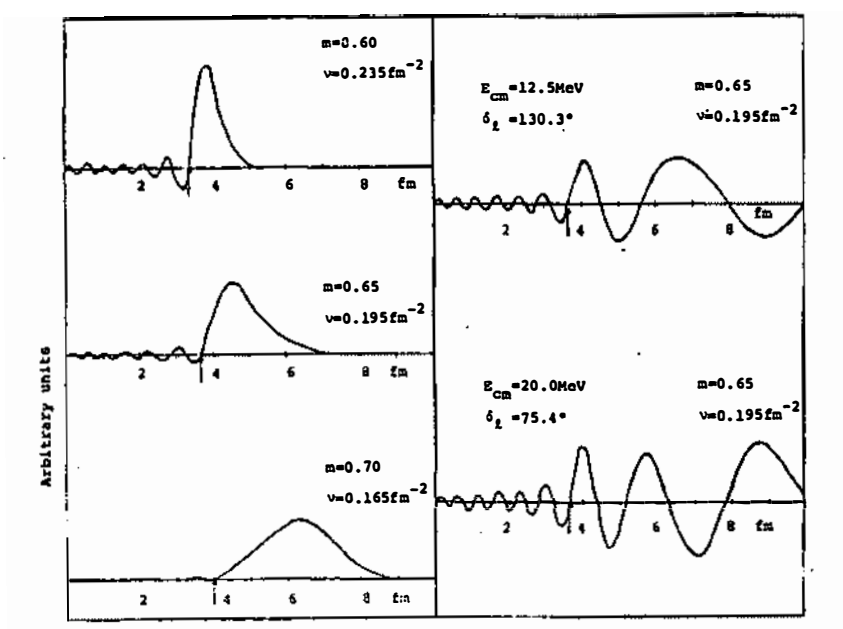

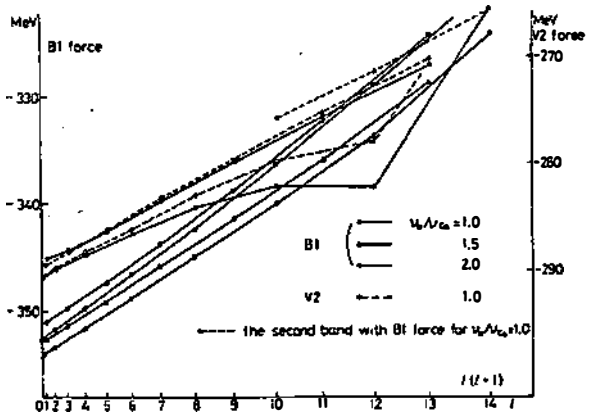

Fig.6 The level scheme of the $\alpha+^{40}Ca$ is shown by the ROM for the general case with different oscillator parameters. The second band for the case with common oscillator parameter is also shown in dashed line with black circles.

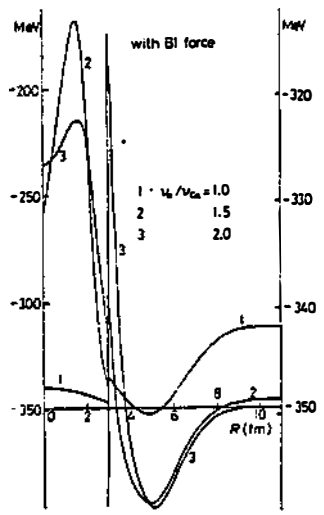

Fig.7 The energy surface with non-projected scheme is illustrated for three cases of the $\alpha+^{40}Ca$.

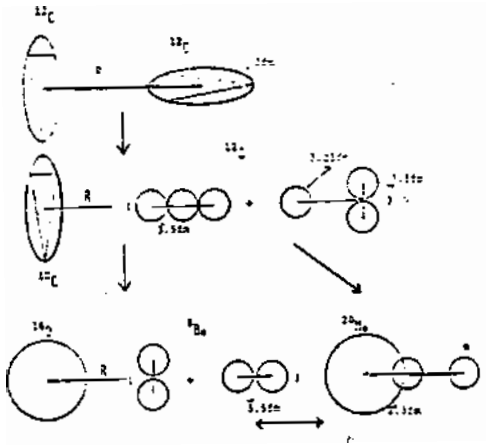

Fig. 8.

Schematic model for the transition from the $^{12}C + ^{12}C^{g}$ to other channels. Intermediate channel $^{12}C + ^{12}C$ is hypothetic.

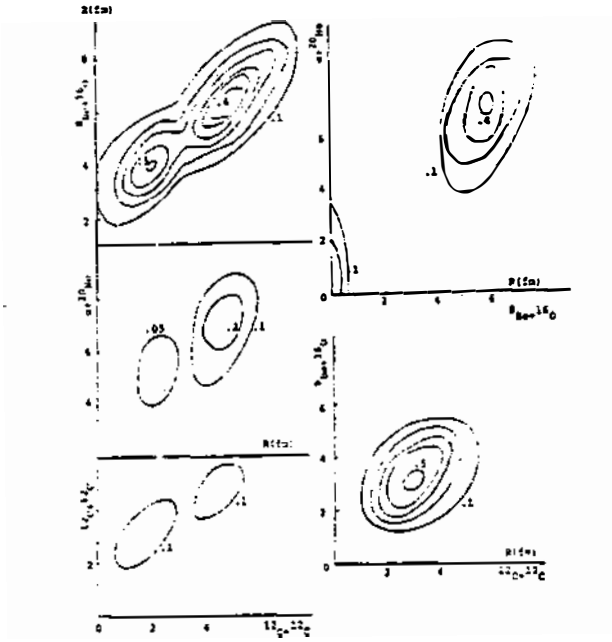

Fig. 9.

The norm kernels between different systems. The case between the $^{12}C + ^{12}C$ and the $\alpha + ^{12}Ne$ is vanishingly small.

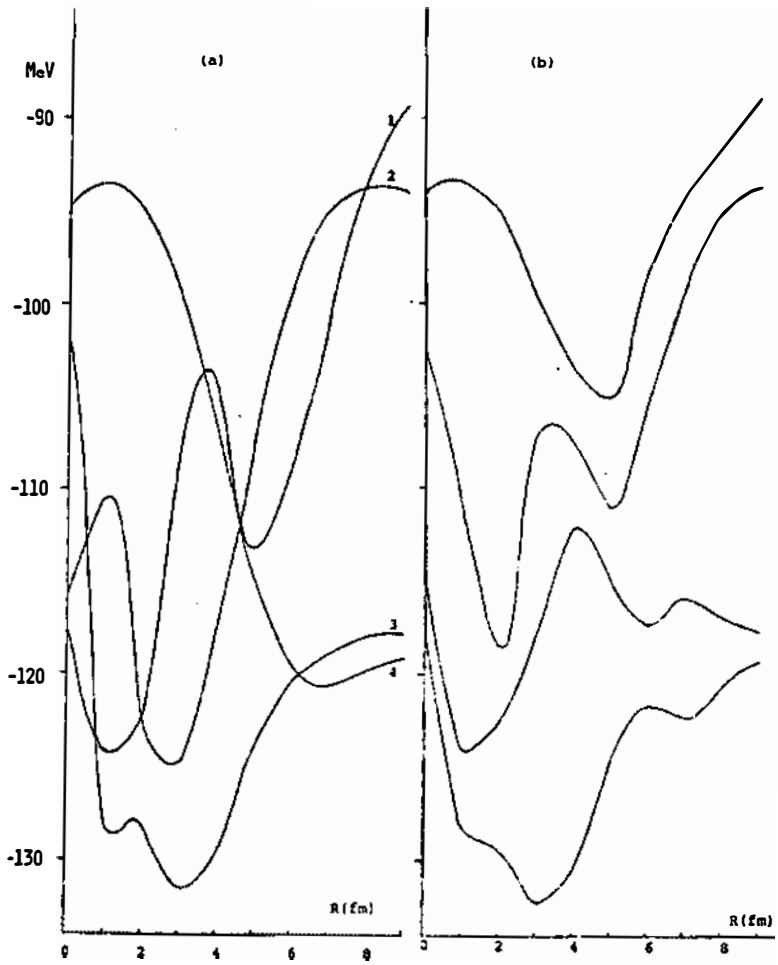

Fig.10 The fast potential is shown in the left side, and is defined by the energy surface for each system. The slow potential is illustrated in another side, and is diagonalized for four systems at fixed R.

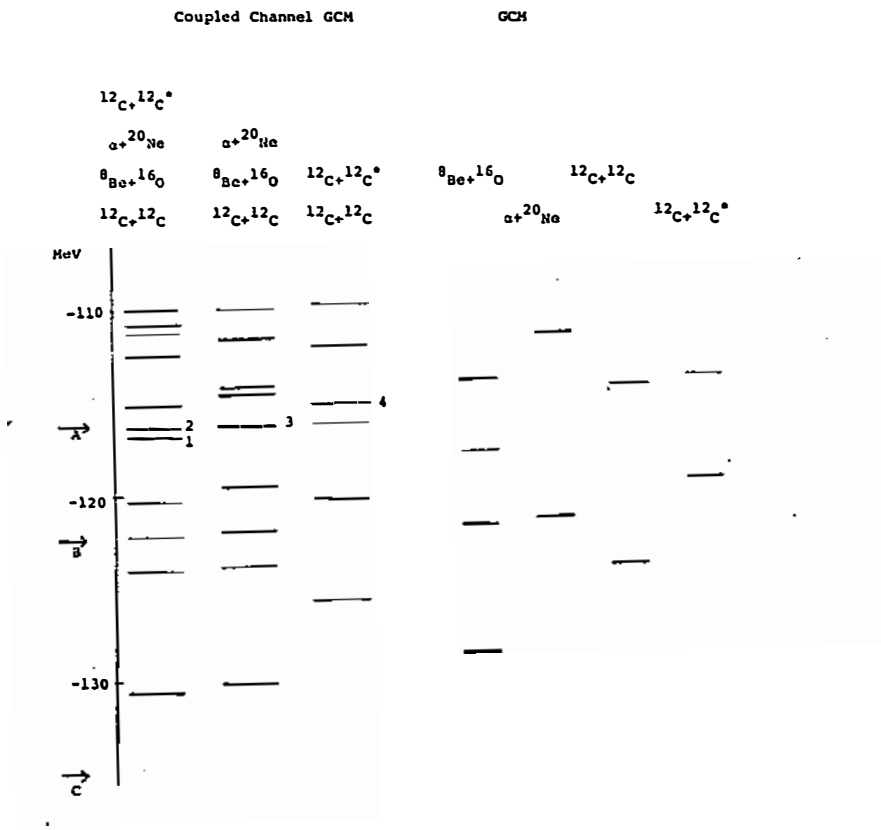

Fig.11 The level structure of the coupled channel GCM. Coupling scheme is written in upper side. The figure in the right side shows the level scheme of each system without coupling.

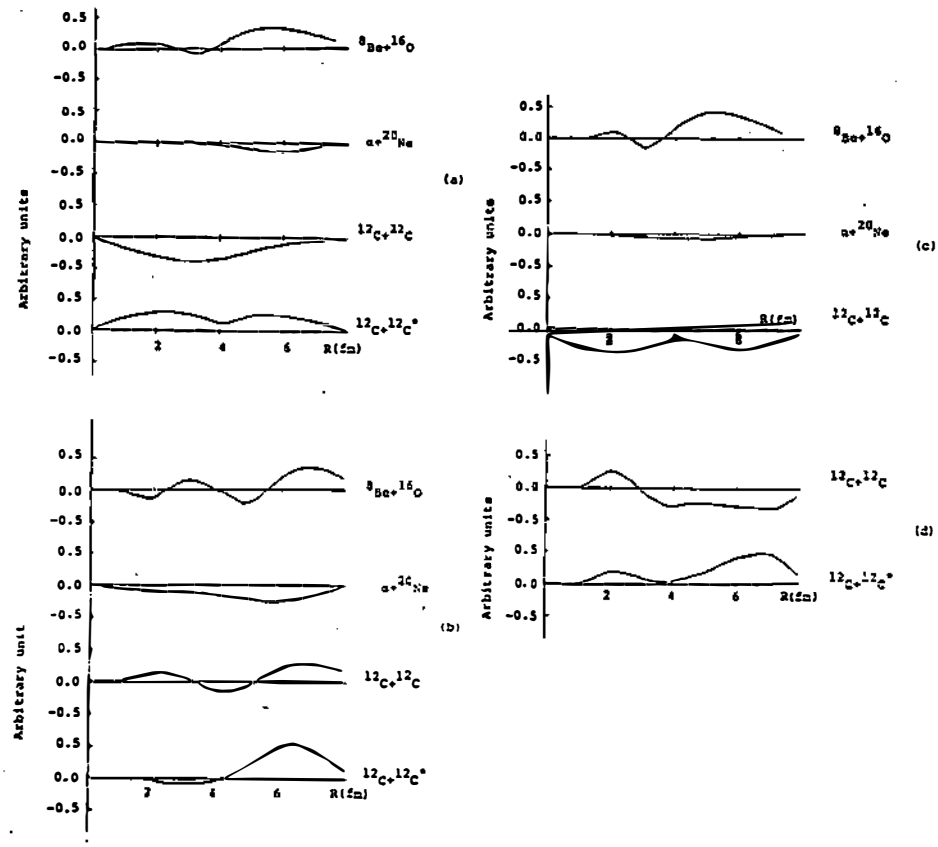

Fig.12 The modified weight function without redundancy corresponds to the level marked in Fig.11.

DISCUSSION

N. Cindro: This comment refers to the transparency where you have shown the structural decomposition of a "molecular state" in ^{24}Mg. It appears that the maximum of the $\alpha\{^{12}C + ^{12}C\} + \sqrt{1-\alpha^2}\{^{12}C + ^{12}C^*\}$ configuration is around 6 fm and that all the other configurations are smaller at that distance. Well, I hope to be able to show this afternoon numbers extracted form experiment that speak in favour of your calculations. (They concern the radius of the $^{12}C + ^{12}C$ system extracted form the experimental E_{exc}(res)vs. J(J+ 1) plot)

A. Tohsaki-Suzuki: I think both the second 0^+ in ^{12}C and the first 2+ with large vibrational-rotational deformation play an important role in molecular resonances of $^{12}C + ^{12}C$ system.

The molecular resonances at 6 fm cannot be explained in terms of the $^{12}C + ^{12}C$ system only because it shows the relative rotational state located at ~3 fm.
Furthermore, our model opens a path from the $^{12}C + ^{12}C$ channel into $\alpha + ^{20}Ne$ and $^{8}Be + ^{16}C$ channels.